Inertial dynamics of pinned charge-density-wave condensates. I. $NbSe_3$

D. Reagor, S. Sridhar, and G. Gruner
Department of Physics and Solid State Science Center, University of California, Los Angeles, California 90024
(Received 28 October 1985)

Conductivity measurements are reported for the linear-chain compound $NbSe_3$ in the frequency range 9–100 GHz. In both charge-density-wave (CDW) states, which develop at $T_1=144$ K and at $T_2=59$ K, a strongly frequency-dependent response is observed with $\mathrm{Re}\sigma(\omega)$ decreasing with increasing frequency. The behavior is described in terms of a harmonic oscillator response, and in the measured spectral range the expression $\mathrm{Re}\sigma_{\mathrm{CDW}}(\omega)=(ne^2\tau/m^*)[1/(1+\omega^2\tau^2)]$ provides an excellent account of our findings. We evaluate the effective mass m^* and damping constant τ from a fit to the above equation. The measured effective mass is only weakly temperature dependent, and in both CDW states is in good qualitative agreement with those determined using the theory of Lee, Rice, and Anderson. We also discuss the temperature-dependent damping constant, and a comparison with data taken in the radio-frequency range is given.

I. INTRODUCTION

The dynamical properties of the electron-hole condensate, called the charge-density wave (CDW) has attracted considerable attention recently.[1] In the absence of damping and pinning the frequency-dependent response of an incommensurate CDW resembles that of a superconductor: The spectrum consists of a collective-mode contribution at zero frequency and a contribution from single-particle excitations across the gap.[2,3] In contrast to a superconductor, pinning potentials interact with the collective mode, which distorts around the pinning centers, due to the absence of a gap in the phason branch.[4] Also, the interaction of the moving condensate with thermally ambient phonons or phasons, and with the uncondensed electrons, leads to damping. Consequently, the oscillator strength is moved from $\omega=0$ to finite frequencies, resulting, for weak pinning potentials, in a strongly frequency-dependent response in the spectral range well below the single-particle gap.

Because the condensate is a strongly coupled electron-phonon system, the effective mass is large, and is given at zero temperature by[2,3]

$$\frac{m^*}{m_b}=1+\frac{4\Delta^2}{\lambda\omega_{2k_F}^2}\ , \tag{1}$$

where Δ is the single-particle gap, related to the bandwidth D by the BCS expression

$$\Delta=D\exp\left[-\frac{1}{\lambda}\right]\ . \tag{2}$$

In the mean-field approximation λ is the dimensionless electron-phonon coupling constant, and ω_{2k_F} is the unrenormalized phonon frequency at wave vector $q=2k_F$. A typical gap of the order of 3×10^{-2} eV leads to $\lambda\simeq0.3$. Then, a typical phonon frequency of 50 K leads to an effective mass $m^*/m_b\simeq400$ significantly larger than the free-electron mass.

Pinning, for an incommensurate CDW, is due to impurities which interact with the collective mode; this has been treated in detail by Fukayama and Lee[4] and by Lee and Rice.[5] This leads to a finite phase-phase correlation length L_0, and the average pinning frequency is given by the standing wave phason oscillations corresponding to the wave vector $q=2\pi/L_0$. Consequently,

$$L_0=\frac{c_0}{\omega_p}=\left[\frac{m_b}{m^*}\right]\frac{v_F}{\omega_p}\ , \tag{3}$$

where $c_0=(m_b/m^*)v_F$ is the phason velocity. Although elaborate estimates of L_0 in terms of the pinning potentials and of the elastic constant associated with the condensate are possible,[1] a typical impurity concentration of $c=100$ ppm leads, for strong pinning in one dimension, to a typical distance of $L_0=a_0/c\simeq10^{-4}$ cm, where a_0 is lattice constant. Then, with $v_F=3\times10^7$ cm/sec and our previous estimate of m^*/m_b, $\omega_p\simeq10^9$, i.e., the characteristic pinning frequency is in the microwave region. At this frequency and above, the maximum conductivity is determined by the damping and given by

$$\sigma_{\max}=\frac{ne^2\tau}{m^*}\ , \tag{4}$$

where n is the number of condensed electrons and τ is a phenomenological damping constant. Equation (4) also describes the conductivity obtained at high electric fields. As a rule, the high-field and high-frequency conductivities approach the values which are obtained in the metallic region, just above the phase transition where the CDW develops, and where the conductivity can be described in terms of the single-particle expression $\sigma=ne^2\tau_n/m_b$. Consequently,

$$\tau/m^*\simeq\tau_n/m_b\ , \tag{5}$$

and with a typical relaxation time $\tau_n^{-1}\simeq10^{-14}$ sec and m_b the free-electron mass, our previous estimate suggests that $1/\tau\simeq2.5\times10^{11}$, and the characteristic frequency for a

high-frequency roll-off is in the millimeter-wave spectral regime.

The above estimations suggest that in typical materials, i.e., $NbSe_3$ and TaS_3, strongly frequency-dependent conductivity is expected below the far infrared. The dc conductivity is zero, and rises with increasing frequency up to $\omega=\omega_p$, followed by a Drude-like decrease at frequencies $\omega\simeq 1/\tau$.

A large body of experimental investigations[6-13] have focused on the low-frequency end of the spectrum, and the frequency-dependent conductivity

$$\sigma(\omega)=\mathrm{Re}\sigma(\omega)+i\,\mathrm{Im}\sigma(\omega)$$

is well explored in a wide range of materials. Because of the limited spectral range (9 GHz and below) the high-frequency part of the collective CDW conductivity spectrum has not been measured. Consequently, the fundamental parameters of the problem, the effective mass, the pinning frequency, and damping constant have not been evaluated on experimental grounds. To emphasize this point we mention that, for a description of $\sigma(\omega)$ in terms of a classical harmonic oscillator response, the measured conductivity indicates overdamped collective motion where the single parameter being measured is $\omega_0^2\tau$, the so-called crossover frequency. ω_0 and m^* cannot be evaluated, resulting in a large variation in the values used to account for different experimental findings.

In this, and in the following paper[13] (hereafter referred to as II) we present detailed frequency-dependent conductivity studies in the spectral range of 10—100 GHz, in the model compounds $NbSe_3$, in both CDW phases, and in *o*-TaS_3 (orthorhombic TaS_3). The expanded frequency scale allows us to study the inertial dynamics of the collective mode, and—by also including experimental results obtained at lower frequencies and reported earlier—all the fundamental parameters of the problem, together with their temperature dependence, are evaluated. The measured effective-mass values are in good qualitative agreement with the mean-field theory of CDW dynamics. The damping constants compare favorably with the recent theory of Takada *et al.*[14] although the temperature dependence is different. Preliminary results were reported earlier.[15,16]

II. EXPERIMENTAL METHOD AND RESULTS

The materials used in this study were prepared by the technique of vapor deposition as described in earlier publications.[17] The starting materials were high purity Nb and Se obtained from commercial suppliers. For the two $NbSe_3$ preparations used in this study the ratio of the room-temperature dc resistivity to the dc resistivity at 4.2 K was 150 to 200. Many of the frequency-dependent conductivity measurements were performed on both preparations, and the results were consistent to within the error bars shown in the figures. The dc conductivities were measured with standard four-probe techniques.

The conductivities at 9 and 35 GHz were measured with the resonant cavity technique of Buravov and Schegolev.[18] A block diagram of the apparatus is shown in Fig. 1. The frequency of the oscillator was swept through

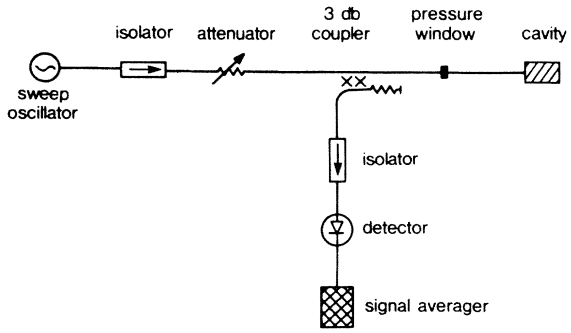

FIG. 1. A block diagram of the apparatus used for the resonant cavity measurements at 4.5, 9, and 35 GHz.

the resonant frequency of the cavity, and the power reflected from the cavity was directed by a circulator to a diode detector. Both cavities were operated in a TE_{011} mode with the sample at an antinode of the electric field. A multichannel signal averager was used to record a large number of sweeps and subtract a baseline. The cavities were placed in a Dewar and separated from the cryogenic liquids by a stainless-steel tube. The tube was filled with exchange gas to ensure equilibrium between the diode thermometer, which was outside the cavity, and the sample.

The resonance was recorded with and without the sample and the change in the resonance was characterized by the change in center frequency, δ, and the change in the full width of the resonance at half height, Δ, both normalized to the resonant frequency. The complex dielectric function is given by $\epsilon=\epsilon'-i\epsilon''$, where[18]

$$\epsilon'-1=\frac{1}{N}\frac{\delta(\alpha/N-\delta)-(\Delta/2)^2}{(\Delta/2)^2+(\alpha/N-\delta)^2}\ , \tag{6a}$$

and

$$\epsilon''=\frac{\alpha}{N^2}\frac{\Delta/2}{(\Delta/2)^2+(\delta-\alpha/N)^2}\ . \tag{6b}$$

Here, α is the filling factor, and N is the depolarization factor of the sample. The absolute complex dielectric constant can therefore be determined if α and N are known. For a cylindrical cavity, a TE_{011} mode, and the sample position used at both frequencies, the filling factor is given by

$$\alpha=2.1V_s/V_c\ , \tag{7}$$

where V_s is the volume of the sample and V_c is the volume of the resonant cavity. For a long slender ellipsoidal sample the depolarization factor is given by[19]

$$N=\frac{ab}{L^2}\left[\ln\left[\frac{4L}{a+b}\right]-1\right]\ , \tag{8}$$

where a and b are the transverse dimensions, L is the length, and $L\gg a,b$. If the sample is approximated as an ellipsoid, then Eq. (8) may be used to estimate the depolarization.

The parameters α and N may be determined from the geometry of the sample, as discussed above, but more ac-

curate values may be obtained from the experimental data or appropriate normalization of the results. To illustrate the determination of the unknown parameters α and N from the raw data we define the complex resonant frequency shift $\delta\omega/\omega=\delta+i\Delta/2$ and invert Eqs. (6a) and (6b) to obtain

$$\frac{\delta\omega}{\omega}=\frac{-\alpha(\epsilon-1)}{1+N(\epsilon-1)} . \tag{9}$$

The complex conductivity is given by $\sigma=i\omega\epsilon/4\pi$. If $\mathrm{Re}\sigma$ becomes large, then $\mathrm{Im}\epsilon$ also diverges and the frequency shift is real (lossless) and equal to $-\alpha/N$. If the sample being measured has a highly conducting limit, as is the case for $NbSe_3$ at low temperatures, then α/N is directly determined from the measured shift, δ. A second equation is necessary to determine α and N independently. This is obtained by normalizing $\mathrm{Re}\sigma$ to the dc conductivity at room temperature. For the TaS_3 measurements discussed in the companion paper[13] the conductivity does not reach a highly conducting limit and α/N cannot be measured directly. Two equations to determine the parameters α and N may be obtained, in this case, by normalizing the ac conductivity to the dc conductivity at room temperature, exactly as for $NbSe_3$, and setting $\epsilon'=0$ at room temperature. This assumes that CDW effects at room temperature are negligible (i.e., the material is a normal metal) in comparison to the large effects below the phase transition.

The above relations between cavity parameters and conductivity are derived in the quasistatic limit. This assumes that the classical skin depth is comparable to or larger than the sample. When the skin depth is smaller than the sample, a regime known as the skin-depth limit, δ is still equal to $-\alpha/N$ but Eq. (9) no longer applies for the determination of Δ. In the $NbSe_3$ measurements the large conductivity at low temperatures places the measurements near the skin-depth limit. It is difficult to distinguish between the two conditions so we terminate the data set when the shift saturates and take this saturated value as $-\alpha/N$. In practice this resulted in discarding the conductivity measurements below 25 K.

The measurements performed at 30 GHz, 60 GHz, and higher frequencies were performed with a millimeter-wave bridge technique developed by the authors.[20] Three bridges were built covering the Ka (26–40 GHz), V (50–75 GHz), and W (75–110 GHz) bands. The bridges were essentially identical and are depicted in block diagram form in Fig. 2. The millimeter-wave sources used were both Gunn diodes and Impatt diodes from Hughes Aircraft Co. The Impatt diodes were stabilized with a source locking counter. Power from the oscillator was chopped by the modulator, split at the first "T" junction and directed down the reference and sample arms. The wave traveling the reference arm was reflected from a fixed short. In the sample arm the wave was reflected from the impedance to be measured. The waves from the two arms were combined in the second T junction and the output was detected by the diode. The bridge was nulled by adjusting the attenuator and phase shifter such that the power at the detector was zero. For temperature-dependent measurements, the section of waveguide containing the sample was cooled with a helium-gas-flow system to a lowest temperature of approximately 15 K.

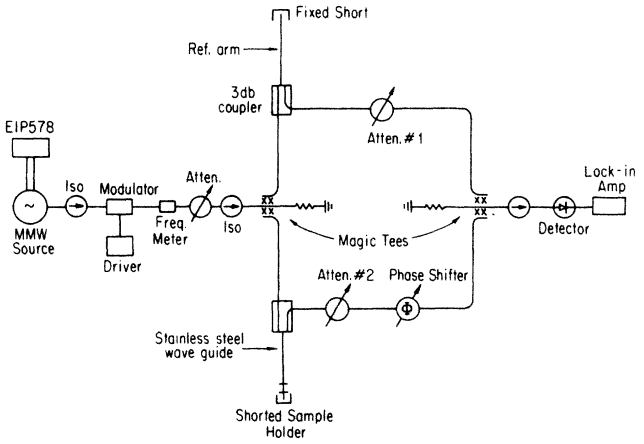

FIG. 2. A block diagram of the millimeter-wave bridge used for the 32-, 60-, 90-, and 109-GHz conductivity measurements.

An unknown impedance was measured by terminating the sample arm with a short and noting the attenuator and phase readings when the bridge is nulled. Then the short was replaced by the unknown impedance and the null settings noted again. The unknown impedance is then

$$\frac{Z}{Z_0}=\frac{1+S}{1-S} , \tag{10}$$

where $S=-10^{-A_S/20}e^{i\phi_s}$ and A_s and ϕ_s are the change in attenuation and phase readings when the replacement is made. The impedance is referred to the plane of the short. If another reference plane, a distance l from the short, is chosen then S is transformed by multiplying by $e^{i4\pi l/\lambda_g}$. This factor results from the phase change over a distance $2l$. Equation (10) is not changed by the transformation.

For conductivity measurements the samples were placed in the center of the sample-arm waveguide a distance $3\lambda_g/4$ from a terminating plate, where λ_g is the guided wavelength. The samples were single fibers 2–3 mm long and $\approx 1\ \mu m^2$ in cross section and aligned with the long axis (CDW axis) parallel to the electric field. With no sample the terminating plate formed a short. The sample was placed in the waveguide through a small hole, and Eq. (5) was used to calculate Z from the measured change in A_s and ϕ_s. The "sample out" and "sample in" measurements were made in separate coolings with the sample added at room temperature.

The sample acts as a dielectric post in the waveguide and several solutions for the impedance of such an obstacle are available.[21,22] In general, the equivalent circuit for the configuration used is a T circuit. However, the impedances in the T arms are smaller by a factor $(d/\lambda)^2$ than the shunt impedance, Z_s. Since the sample diameter d is 1 μm for our samples and λ is 3–10 mm, the circuit is effectively a pure shunt. The shunt impedance is given by

$$Z_s = iX_\infty + Z_\epsilon \,, \tag{11}$$

where X_∞ is the purely inductive reactance of an infinitely conducting and geometrically identical wire at the same position as the sample. In the limit where the classical skin depth is greater than d, Z_ϵ is given by

$$Z_\epsilon/Z_0 = -i\frac{C}{\epsilon - 1} \,, \tag{12}$$

where $C = a/\lambda_g(\lambda/\pi d)^2$ and a is the height of the waveguide.

The above relations are for the case were the sample is in contact with the waveguide walls. In practice, it may be possible to make the sample long enough to traverse the waveguide, but it is impractical to ensure contact with the walls. For infinitely conducting samples the gap between the sample and the waveguide may be modeled as a capacitive impedance in series with the inductive shunt impedance.[23] To obtain the correct limit for high conductivities we must add this capacitive impedance to X_∞. The relative importance of the capacitive and inductive impedances is determined by sample size, with the inductance dominating for long samples completely traversing the waveguide and the capacitance dominating for shorter samples. The interplay of these two effects was studied by varying sample size. For the present experiments, the calculation of X_∞ is difficult and unnecessary because X_∞ could be determined from the raw data.

The functional form relating ϵ and $(jZ_s)^{-1}$, Eqs. (11) and (12), is identical to the relation between ϵ and $\delta\omega/\omega$ in the cavity measurements. The geometric constants in the waveguide analysis could therefore be determined from the same techniques used in the cavity case. If the sample had a highly conducting limit at some temperature, then Z_ϵ becomes negligible and $Z_s = iX_\infty$. The measured impedance in the highly conducting limit then determined X_∞. The second constant, C, was then determined by normalizing to the room-temperature dc conductivity. If the material being measured did not have a highly conducting limit, then a second relation for X_∞ and C was obtained by setting $\epsilon' = 0$ at room temperature.

Tests of the millimeter-wave bridge technique were performed on quartz rods, gold wires, and $TaSe_3$, a test material with a frequency-independent conductivity. The results of the first two tests were consistent with Eqs. (11) and (12) and are discussed in Ref. 20. The dc conductivity of $TaSe_3$, measured four-probe, changed by a factor of 50 over the temperature range of the measurements. The millimeter-wave conductivity measurements were performed at 109 GHz. The sample did not completely traverse the waveguide and the capacitive part of Z_∞ dominated the inductive part. This can be seen from raw data displayed in Fig. 3(a); the phase shift ϕ_s is always negative, characteristic of a capacitive response. At low temperatures, where the conductivity is large the shift saturates and ϕ_∞ is taken to be $-85°$. The choice of $-85°$ is more apparent if the data is plotted in the impedance plane and extrapolated to $\mathrm{Re}(Z) = 0$. The intercept with the imaginary axis is then X_∞ and $X_\infty = \cot(\phi_\infty/2)$. The attenuation is also displayed in Fig. 3(a). It increases sharply, with increasing temperature, at low temperatures

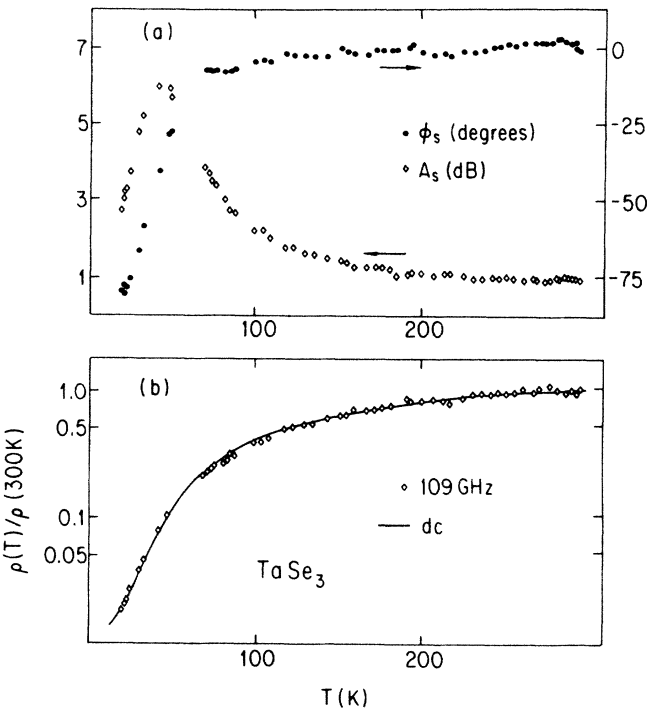

FIG. 3. (a) The change in attenuation and phase shift readings of the millimeter-wave bridge due to a sample of $TaSe_3$. A calibration has been subtracted from the measured attenuation and phase shift to give the results shown. (b) The 109-GHz and dc resistivities of $TaSe_3$. The millimeter-wave resistivity was calculated from the results shown in (a).

to a peak at approximately 40 K then decreases at higher temperatures. The peak results from the depolarization of the sample and a similar peak is often observed in the loss measured in cavity experiments. The millimeter-wave conductivity calculated with Eqs. (11) and (12) is displayed in Fig. 3(b). The results are normalized to the dc conductivity at room temperature and agree with the dc conductivity to within $\pm 10\%$ over the entire range of temperatures. Imσ may also be calculated and it is zero to within the experimental error. The experimental error, however, is large because when $\sigma(\omega)$ is large $iX_\infty \simeq \mathrm{Im}Z_s$ in Eq. (11) and the subtraction results in a large error in $\mathrm{Im}Z_\epsilon$. In the high conductivity limit of Eq. (12), Imσ has a strong dependence on $\mathrm{Im}Z_\epsilon$ and consequently there is a large error in Imσ. Similar tests, not discussed here, were performed for the cavity perturbation technique.

The resistivity of $NbSe_3$ measured at dc and at four different frequencies in the microwave and millimeter-wave spectral range are displayed in Fig. 4. The dc conductivity has the characteristic[6] double-peak structure, and the increase at $T_1 = 144$ K and $T_2 = 59$ K signal the development of the independent charge-density waves which remove part of the Fermi surface. Various analyses based partially on the dc conductivity shown in the figure indicate that approximately 20% to 30% of the carriers are removed by the first phase transition with another 40% to 60% removed below T_2.[24] The two independent CDW's below T_2 show up in both the structural properties and the dynamics of the collective mode, leading to two dif-

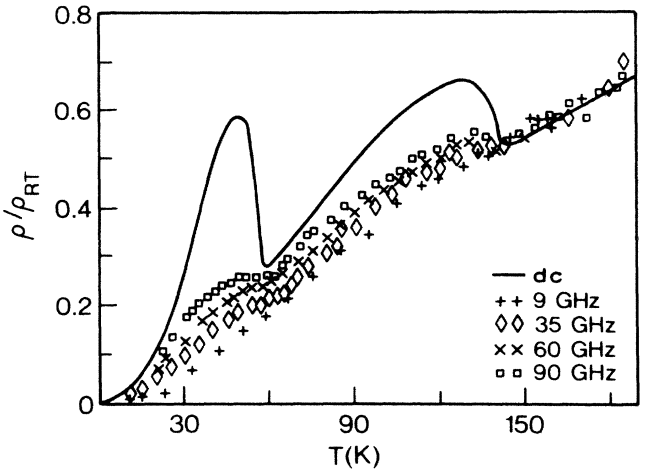

FIG. 4. Normalized resistivity versus temperature for $NbSe_3$ at dc, 9, 35, 60, and 94 GHz.

ferent threshold fields, E_T, for the onset of nonlinear conduction, and consequently two different pinning frequencies, owing to the strong relation between E_T and ω_0. In strong contrast to the dc resistivity, the resistivity measured at 9 GHz shows little evidence for the phase transition, and the conductivity smoothly decreases with decreasing temperature. Our measurements at this frequency are in agreement with the earlier studies,[6] which provided the first clear evidence for a strongly frequency-dependent conductivity of pinned CDW condensates.

We also note that the resistivity, in general, increases with increasing frequency in the spectral range measured. The same data, replotted as conductivities, are displayed in Fig. 5. Without a detailed analysis two features are immediately apparent. First, the decreasing conductivity with increasing frequency is in clear contrast to the increasing conductivity observed below 9 GHz. This behavior suggests an inertial response and a Drude type of roll-off, or alternatively, a depletion of the available density of states at frequencies in and above the millimeter-wave spectral range. This also sets the pinning frequency

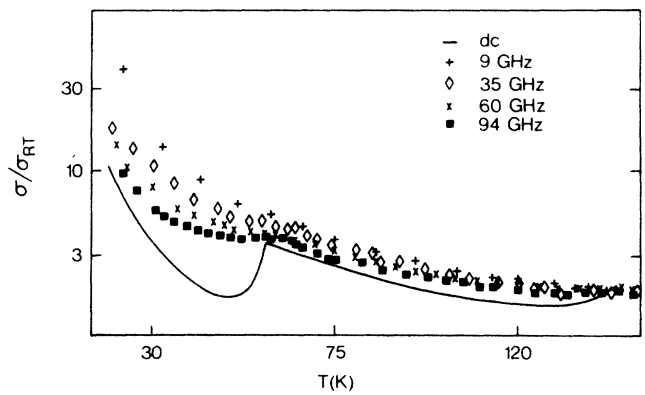

FIG. 5. Normalized conductivity versus temperature for $NbSe_3$. The results displayed are the same as those shown in Fig. 4.

in the microwave region. Second, at temperatures well below the phase transitions, the temperature dependence of the dc and 9-GHz conductivities are rather similar; they, independent of the temperature, differ only by a multiplicative constant. Furthermore, the multiplicative constant is between 1 and 2 in the upper phase and approximately 4 in the lower phase, roughly corresponding to the ratio of the CDW carrier density to the normal carrier density in the respective phases. The numerical constant is therefore of order unity, and Eq. (5) is closely obeyed. Imσ could in principle, be determined but the large conductivities in $NbSe_3$ make the experimental error larger than the measured values (see the discussion of the test results for $TaSe_3$).

III. ANALYSIS

Although it has been suggested that the pinned CDW should have a zero dc conductivity and an ω-dependent response well below the single-particle gap, several distinctly different models have been proposed to account for the frequency-dependent conductivity. Early calculations, which neglected damping, but estimated a distribution of pinning frequencies, led to a high-frequency roll-off at frequencies above the average pinning frequency with a ω-dependent response given by[4]

$$\sigma(\omega)=(\omega'/\omega)^4 . \tag{13}$$

Such a distribution is neglected in a model where the condensate dynamics are treated as that of a classical particle. For small amplitude displacements the equation of motion is[3,25]

$$\frac{d^2x}{dt^2}+\frac{1}{\tau}\frac{dx}{dt}+\omega_0^2 x=\frac{eE}{m^*} , \tag{14}$$

where τ is a phenomenological damping constant and ω_0 is the pinning frequency discussed above. Equation (14) leads to a frequency-dependent conductivity

$$\begin{aligned}\mathrm{Re}\sigma(\omega)&=\sigma_n+\mathrm{Re}\sigma_{\mathrm{CDW}}\\&=\sigma_n+\frac{ne^2\tau}{m^*}\frac{\omega^2/\tau^2}{(\omega_0^2-\omega^2)^2+\omega^2/\tau^2} ,\end{aligned} \tag{15}$$

where it is assumed that the normal and condensed electrons provide two separate channels for the conduction process. Equation (15) has been widely used to describe the ω-dependent response in the radio-frequency spectral range. Such studies have also confirmed that, within the framework of this description, the response is overdamped, and the crossover frequency $\omega_0^2\tau \ll \omega_0$. As may be seen from Eq. (15), the crossover frequency is given as the frequency where the $\mathrm{Re}\sigma_{\mathrm{CDW}}$ is half of the maximum conductivity. We note, however, that an alternative description[26] also provides an excellent fit in this frequency region.[11] Both imply a broad plateau of $\mathrm{Re}\sigma(\omega)$ near the resonant frequency. Our experiments performed at 9 GHz are also in agreement with those performed below this frequency. Consequently, we conclude that the conductivity measured at 9 GHz is close to the conductivity $\mathrm{Re}\sigma(\omega_0)$.

Figures 6 and 7 display the conductivity versus fre-

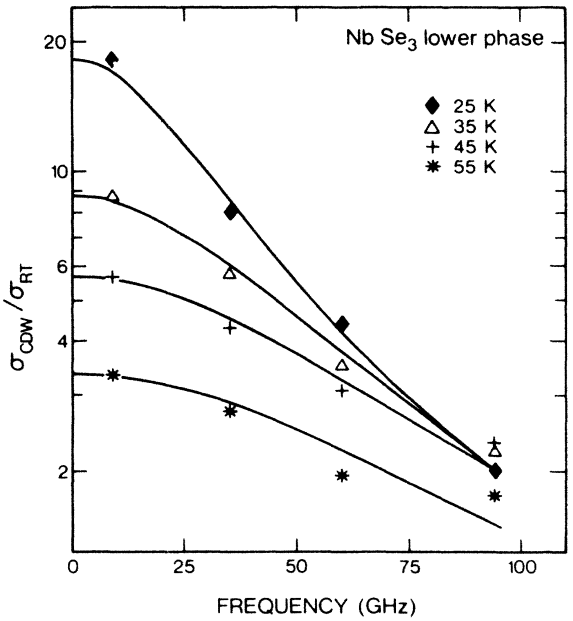

FIG. 6. Conductivity versus frequency at several temperatures in the lower CDW phase of $NbSe_3$. The solid curves shown are a best fit to Eq. (16) at each temperature. The conductivity rise at low frequencies is near zero on this scale and may be neglected when fitting to the high-frequency limit of the response.

quency at several temperatures in both CDW phases. Restricting our discussion to the frequency range 10—100 GHz, we find that $\mathrm{Re}\sigma(\omega)$ smoothly decreases with increasing ω and the functional dependence is less dramatic than implied by Eq. (13). An excellent fit is, however, obtained when the high-frequency limit of the harmonic oscillator response

$$\mathrm{Re}\sigma_{\mathrm{CDW}}(\omega)=\frac{ne^2\tau}{m^*}\frac{1}{1+\omega^2\tau^2}=\sigma_{\max}\frac{1}{1+\omega^2\tau^2} \tag{16}$$

is used. The solid lines are obtained by setting

$$\mathrm{Re}\sigma(9\ \mathrm{GHz})=\mathrm{Re}\sigma(\omega_0/2\pi)=ne^2\tau/m^*$$

and adjusting τ to minimize the error on a linear scale. It is evident that (with the exception of temperatures just above T_2) a Drude-type high-frequency roll-off is in agreement with our experimental findings.

We note that the threshold field for nonlinear conduction[27] increases and the dielectric constant decreases[7] with decreasing temperature well below the transition. This suggests an increasing pinning frequency ω_0 with decreasing temperature. Indeed this is evident in Fig. 6 where at 70 K a fit using Eq. (16) is not possible and we had to revert to Eq. (15) with a finite pinning frequency of $\omega_0/2\pi=15$ GHz. We also note that the fit to Eq. (16) is excellent for the lower-temperature CDW phase, except near T_2; this feature will be discussed later.

The two fit parameters, $1/\tau$ and $\sigma_{\max}=ne^2\tau/m^*$, may be used to calculate m^*/n for the CDW condensate. In addition, well below the phase transition the carrier density n approaches a zero-temperature carrier density, n_0. From the band filling we estimate that the total carrier density is 5.5×10^{21} carriers/cm^3.[24] Using our estimate that 20% of the normal carriers condense at the upper transition and an additional 60% condense at the lower transition, the carrier density n_0 for the upper transition is $0.2(5.5\times10^{21})$ and for the lower transition is $0.8(5.5\times10^{21})$. Using these quantities, we may calculate m^*n_0/nm_e, the effective mass of the condensate relative to the free-electron mass, m_e, at temperatures well below the phase transition. The carrier concentration in the upper phase is not clearly established and may be as large as $0.3(5.5\times10^{21})$, resulting in an increase of m^* by a factor 1.5.

The parameters obtained from the fit are displayed in Figs. 8 and 9 for the lower and upper phases, respectively. In the upper phase the temperature dependences of $1/\tau$ and $\sigma_{\max}$ are large, both vary by a factor of 2, but inversely to each other. When the product is taken, the temperature dependence almost cancels. Using $1/\tau$ and $\sigma_{\max}$, M^*n_0/nm_e was calculated and is also plotted in Figs. 8 and 9. The product is constant within error bars for the upper phase except near the phase transition where a small increase occurs. At temperatures well away from the phase transition the effective mass is approximately 230 free-electron masses. Using the larger value of n_0, $0.3(5.5\times10^{21})$, the effective mass is 345. In the lower phase the behavior is similar, except that the conductivity scale is larger by an order of magnitude. n_0 estimated for the lower phase is much larger so the effective mass is only a factor 3 smaller. The temperature dependence of m^*n_0/nm_e is much weaker than for the conductivity, but it is not constant, increasing over the entire lower phase. The effective mass is approximately 100 electron masses in the lower phase well below the phase transition. Our values for the effective mass may be compared with those

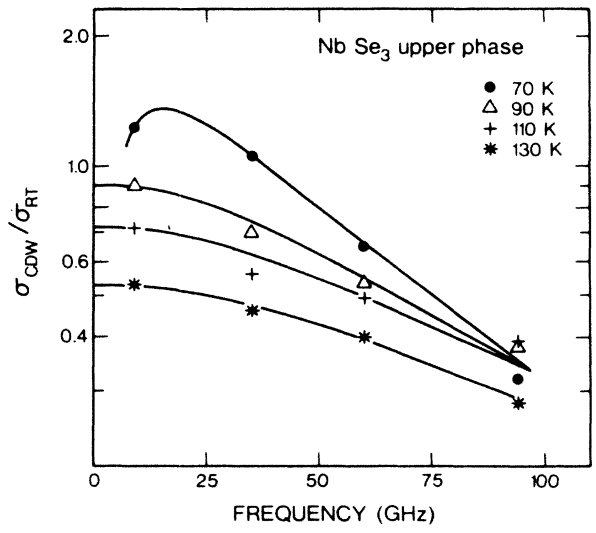

FIG. 7. Conductivity versus frequency at several temperatures in the upper CDW phase of $NbSe_3$. The solid curves shown are a best fit to Eq. (16) at the three higher temperatures. At the lowest temperature the rise from zero conductivity to the maximum begins to enter the frequency range of the measurements and a fit to Eq. (15) is used.

estimated using Eq. (1). Because of the well-established mean-field character of the phase transitions in $NbSe_3$, we use the mean-field expressions, Eq. (2) and $\Delta = 1.76 k_B T_p$, to evaluate λ and Δ. The phonon frequency at wave vector $2k_F$ and in the absence of an electron-phonon interaction, ω_{2k_F}, has not been determined by a direct measurement in this material. In another CDW compound, $K_{0.3}MoO_3$,[28] the phonon dispersion has been measured with neutron scattering, and at temperatures well above the phase transition the measured phonon frequency near $2k_F$ is 1 THz, which corresponds to 50 K in temperature, and does not show any evidence of softening. The measured phonon frequency at $2k_F$ is therefore approximately equal to ω_{2k_F}. In typical materials the Debye temperature, which is comparable to the phonon frequency at $2k_F$, is 100–200 K; however, materials with a lower phonon frequency at $2k_F$ are the materials which will favor a Peierls transition. The low phonon frequency in $K_{0.3}MoO_3$ is therefore not unexpected for a CDW material, and we use the same value of $\omega_{2k_F}[k_B(50\ \text{K})/\hbar]$ for $NbSe_3$. The bandwidth D is difficult to determine for this

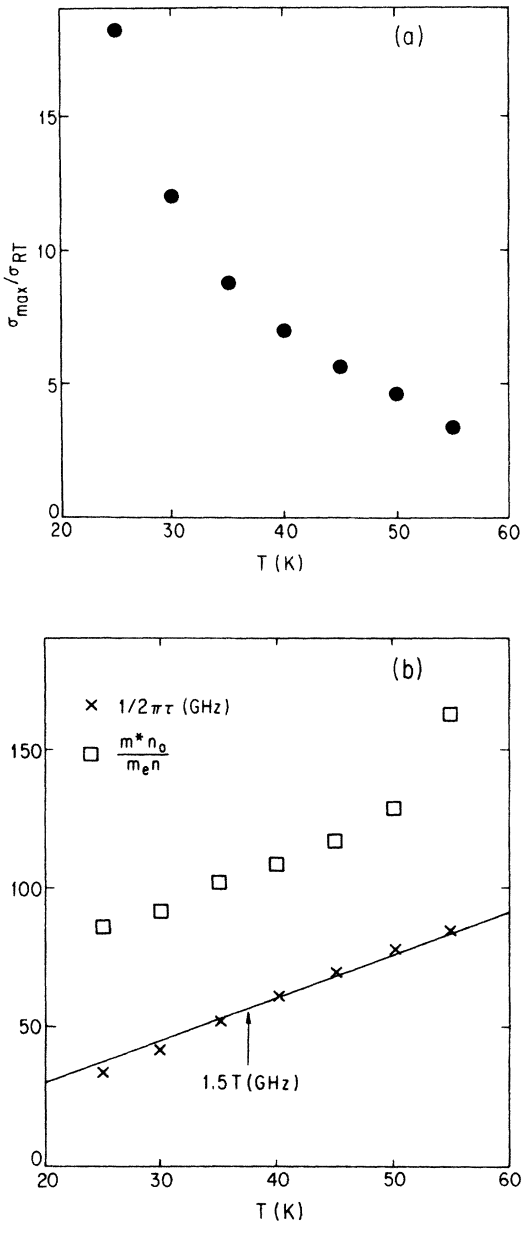

FIG. 8. The parameters derived from the fit of Eq. (16) to the measured conductivity of the CDW in the lower phase. (a) The maximum conductivity normalized to the room-temperature conductivity versus temperature. (b) The damping constant and effective mass versus temperature. At temperatures well below the phase transition the parameter $m^* n_0/m_e n$ is the effective mass of the CDW.

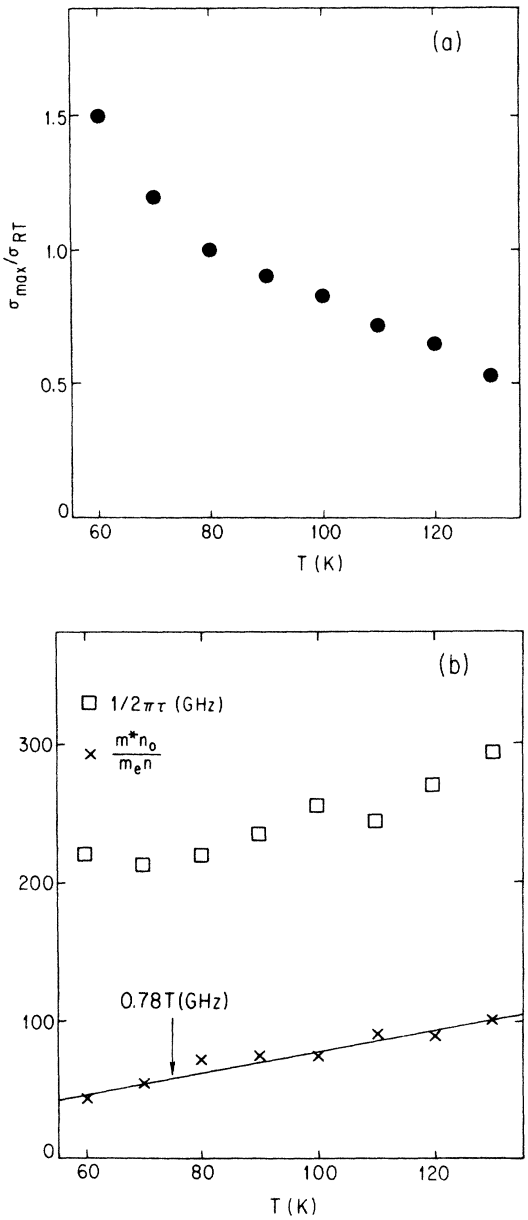

FIG. 9. The parameters derived from the fit of Eq. (16) or (15) to the measured conductivity of the CDW in the upper phase. (a) The maximum conductivity versus temperature. (b) The damping constant and effective mass versus temperature. At temperatures well below the phase transition the parameter $m^* n_0/m_e n$ is the effective mass of the CDW.

material and only enters logarithmically in λ. An adequate estimate is that $D=2\epsilon_F$, where ϵ_F is the Fermi energy, and $\epsilon_F=0.3$ eV is determined from a free-electron model where the effective mass is unity and the wave vector is $2k_F$. This results in an effective mass of 78 in the lower phase and 340 in the upper phase, in good agreement with the measured values. (See Table I of paper II).

The above analysis of the response in the lower phase has assumed that the two CDW's present are strongly coupled and contribute to the effective mass as a single condensate. The x-ray diffraction results,[29] however, indicate two distinct satellite peaks, one associated with each transition. In addition, mean-field behavior should be observed for the temperature dependence of m^*n_0/m_en. Consequently, a model where the two condensates are weakly interacting and move independently will be more appropriate for the lower phase. To estimate the effective mass of the lower phase condensate in a model with two independent CDW's several extrapolations of the upper phase conductivity were chosen. The extrapolated upper phase conductivity, $\sigma^u_{\rm CDW}(\omega)$, was then subtracted from $\sigma_{\rm CDW}(\omega)$ in the lower phase and the resulting conductivity attributed to the CDW condensing at the lower phase transition. The quantity $\sigma^u_{\rm CDW}(\omega)$ is specified by three parameters: $1/2\pi\tau_u$, $\sigma^u_{\rm max}=n_ue^2\tau_u/m_u^*$, and ω_0^u; and by Eq. (15). However, as may be seen in Fig. 9, $m_u^*n_0^u/m_en_u$ saturates at 230 as the temperature is decreasing in the upper phase and the saturated value may be used to relate $\sigma^u_{\rm max}$ to $1/\tau_u$. Therefore $1/\tau_u$ and ω_0^u are the only parameters whose temperature dependence must be extrapolated from the upper phase. Two extrapolations were chosen for the temperature dependence of $1/\tau_u$. The first was using the line fit to the damping in the upper phase and shown in Fig. 9, $1/2\pi\tau_u=T(0.78\ {\rm GHz/K})$. This extrapolation is almost certainly an upper bound on $1/2\pi\tau_u$ because the measured damping at 60 and 70 K is already clearly below the extrapolation. Setting $\omega_0=0$ and using Eq. (15) then completely specifies $\sigma^u_{\rm CDW}(\omega)$. The conductivity in the lower phase, due to the lower-phase condensate only, is then

$$\sigma^l_{\rm CDW}(\omega)=\sigma_{\rm CDW}(\omega)-\sigma^u_{\rm CDW}(\omega)\ . \tag{17}$$

The resulting conductivity at 45 K is shown in Fig. 10 and labeled 1. The solid line is the best fit to Eq. (16) and corresponding to an effective mass of 95. For this extrapolation the response is still overdamped for both condensates and a finite ω_0 for either condensate does not alter the effective mass calculated by more than 10%.

The second method for extrapolating $1/\tau_u$ is derived from the comments associated with Fig. 5; the damping of the CDW in both phases is equal to the damping of the normal electrons to within a numerical factor of order unity, in agreement with Eq. (5). The 9-GHz conductivity directly reflects the temperature dependence of the damping for both CDW's and the normal carriers and may be used to extrapolate the damping, $1/\tau_u$, from the upper phase with the relation, $\tau_u\propto\sigma(\omega/2\pi=9\ {\rm GHz})$. At 45 K this extrapolation results in $1/2\pi\tau_u=30$ GHz. The pinning frequency used in the second extrapolation is now relatively important to properly determine the effective

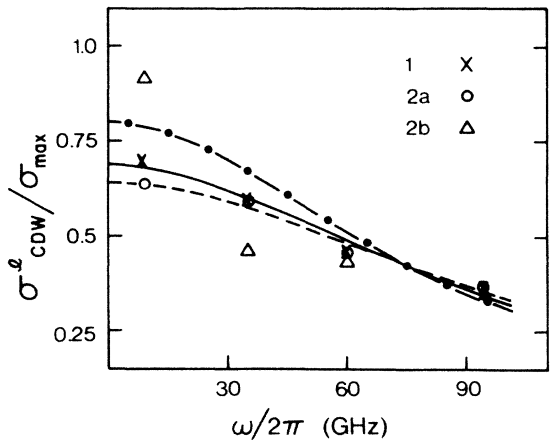

FIG. 10. The estimated conductivity resulting only from the CDW that condenses at the lower phase transition. The three estimates used are discussed in the text. The solid line (——), dashed line (— — —), and the dotted-dashed line (—·—·—·) are best fits to Eq. (16) for estimates 1, 2a, and 2b, respectively. The effective mass is approximately 95 electron masses in all cases.

mass in the lower phase because $\sigma^u_{\rm CDW}(\omega)$ may be underdamped. Two pinning frequencies were chosen at 45 K, zero, and 25 GHz, the latter corresponding to a reasonable upper bound on the pinning frequency. The pinning frequency in the upper phase is increasing as the temperature is decreased and is approximately 15 GHz at the lower phase transition. Extrapolating into the lower phase would result in $\omega_0/2\pi$ greater than 15 GHz. An upper bound of $\omega_0^u=25$ GHz at 45 K is necessary because any larger values of ω_0 would result, through the subtraction in Eq. (17), in negative values of $\sigma^l_{\rm CDW}$ or two peaks in $\sigma^l_{\rm CDW}$, both of which are physically unreasonable. The second extrapolation of τ_u, with $\omega_0=0$ and labeled 2a, and with $\omega_0=25$ GHz and labeled 2b, is also shown in Fig. 10. The best fits to Eq. (16) are the lines in the figure and correspond to $m^*/m_e=92$ for fit 2a and $m^*/m_e=96$ for fit 2b. The effective mass of the lower phase condensate is therefore approximately 95 and depends only weakly on any arbitrary aspects of the extrapolation. The effective mass from the two-fluid model is displayed in Table I of paper II for comparison. This analysis of the results to obtain the effective mass has covered both extremes of charge-density-wave coupling, and in both cases we obtain a lower-phase effective mass in the range 90 to 120 electron masses.

The temperature dependence of the effective mass has been discussed in detail by Rice, Lee, and Cross,[30] who also included the effect of uncondensed electrons. In the absence of these, the temperature-dependent effective mass

$$\frac{m^*}{m_b}=1+\frac{4\Delta^2(T)}{\lambda\omega^2_{2k_F}} \tag{18}$$

and m^*/m_b goes to one at the phase transition within the mean-field approximation. With the number of condensed electrons, $n\propto\Delta^2$ for $T<T_p$, the temperature dependence may be written in the form

$$\frac{m^*}{m_b}=1+\frac{4\Delta^2(0)}{\lambda\omega_{2k_F}^2}\frac{n(T)}{n(T=0)} . \tag{19}$$

Consequently the relation

$$\frac{m^*}{n}\frac{n(T=0)}{m_b} \tag{20}$$

is independent of temperature. The above formulas are appropriate when the dynamics of the condensed electrons and that of the normal electrons are decoupled. Such decoupling is suggested by conventional treatments of the nonlinear dc conductivity and also other transport coefficients like the thermoelectric power[31] and the Hall effect,[32] and also by the strictly linear relation between the current oscillations and the excess nonlinear current. The analysis of the above phenomena is performed by assuming that

$$\sigma=\sigma_n+\sigma_{\rm CDW} , \tag{21}$$

where σ_n refers to the conductivity due to the uncondensed electrons. Such decoupling, however, may not be appropriate near the phase transition as discussed by Gorkov and Dolgov.[33] In this case the temperature-dependent effective mass is determined by the coupled response to the normal and uncondensed electrons. The effective mass at $T=0$ is identical to that of Eq. (1) but near T_p (Ref. 30):

$$\frac{m^*}{m_b}=1+\frac{T_p^2}{\lambda\omega_{2k_F}^2} \tag{22}$$

and, in contrast to Eq. (18), remains finite at the phase transition. Consequently the ratio given by Eq. (20) diverges at $T=T_p$. It should be mentioned, however, that the mean-field treatment is expected to break down as T approaches T_p from below, just where the difference between the two effective masses becomes most important.

In the upper phase our measured temperature dependence appears to lie between the two limits discussed by Rice *et al.*[30] The ratio given by Eq. (20) increases with increasing temperature. This increases, however, is too weak near the phase transition to be described using Eq. (22). In the lower phase the temperature dependence of the effective mass could be an artifact introduced by modeling the response as that of a single condensate.

The question of damping has also been addressed,[14,33–35] but no detailed theory which takes the effect of normal electrons into account is available at present. Qualitative arguments of why Eq. (5) may be approximately correct have been advanced by Bardeen.[35] It has also been shown[33] that near the phase transition

$$\sigma_n+\sigma_{\rm max}=\frac{n_n e^2\tau_n}{m_b}+\frac{ne^2\tau}{m^*}\simeq\frac{n_0e^2\tau_0}{m_0} , \tag{23}$$

where n_0, τ_0, and m_0 refer to the number of electrons, the scattering time, and band mass just above the phase transition. This is confirmed by our (and also by previous[6]) experiments which indicate that the conductivity at microwave frequencies (i.e., close to $\omega=\omega_0$) continues to decrease while going through the phase transitions, as should be expected in the absence of phase transitions. The experimental results, presented in Figs. 4 and 5, also indicate that it is approximately obeyed even well below the phase transitions, if n_0, τ_0, and m_0 refer to quantities which would be observed at the same temperature if the material would remain a metal with the Fermi surface not removed. The conductivity reflects the combined temperature dependence of the various parameters involved. The temperature dependence of the inverse relaxation time for both CDW states is shown in Figs. 8 and 9. An approximate linear temperature dependence

$$\frac{1}{2\pi\tau}=AT \tag{24}$$

is observed in both charge-density-wave states, and it is also evident that the coefficients for the upper phase, A_u, and the lower phase, A_l, have the ratio

$$\frac{A_u}{A_l}=\frac{1.5}{0.78}\simeq 2 , \tag{25}$$

which is proportional to the number of condensed electrons in the two phases

$$n_{\rm CDW}(u)/n_{\rm CDW}(l)=0.6n_0/0.3n_0\simeq 2 .$$

Whether this is accidental or not remains to be seen; it is clear, however, that damping associated with the dynamics of the collective mode is a major unresolved question.

Finally, the millimeter-wave results reported here can be combined with earlier results at lower frequencies. The frequency-dependent conductivity over 5 orders of magnitude in frequency and at $T=42$ K is shown in Fig. 11(a).[36] The dashed curve in the figure is a fit to the classical single oscillator model Eq. (15) with parameters $\omega_0/2\pi=6$ GHz, $1/2\pi\tau=70$ GHz, and $\sigma_{\rm max}=25\,000$ $(\Omega\,{\rm cm})^{-1}$. In the lower phase, Fig. 11(a), the crossover frequency deduced from where Reσ is half of the maximum conductivity is 500 MHz. As discussed earlier Imσ could not be determined at microwave and millimeter-wave frequencies, but the lower-frequency measurements yield both Reσ and Imσ. As indicated in Ref. 7 and Table I of paper II, Imσ has a peak near 100 MHz at $T=42$ K, and within the classical model, Eq. (14), this should also be the crossover frequency. This leads to some ambiguities in the fit to the classical model and the evaluation of ω_0, but does not affect the evaluation of m^* or $1/\tau$. The large difference between the values of $\omega_0^2\tau$ deduced above could also be evidence for a two-condensate model in the lower phase. In the upper phase at 130 K, Fig. 11(b), the measurements reported here are combined with measurements from Ref. 37. The dashed curve is a fit to Eq. (15) with parameters $\omega_0/2\pi=3$ GHz, $1/2\pi\tau=100$ GHz, and $\sigma_{\rm max}=2100$ $(\Omega\,{\rm cm})^{-1}$. The large error bars in the figure result from subtracting the large dc component of the upper-phase conductivity. The error bars for the measurements below 1 GHz are taken from Ref. 37.

The classical model fits the results in Fig. 11 qualitatively, but does not agree in detail. In particular, the measured frequency dependence is considerably broader, indi-

cating that the system contains a distribution of pinnings rather than a single oscillator. This deviation is largest at frequencies below 100 MHz, where the harmonic oscillator model predicts $\mathrm{Re}\sigma \propto \omega^2$ and the results indicate that $\mathrm{Re}\sigma$ increases as ω^α, with $\alpha < 1$. In the inertial regime the results do not indicate any broadening of the response beyond the harmonic oscillator model.

The solid curve in Figs. 11(a) and 11(b) is a fit to a second model with a distribution of oscillators where the distribution is in the center frequency of the response, ω_0, and is given by

$$P(\omega_0)=\frac{2}{\pi\omega_c}\frac{1}{1+(\omega_0/\omega_c)^2}\ , \tag{26}$$

where ω_c is the frequency where the distribution is cut off. The frequency-dependent conductivity is then given by

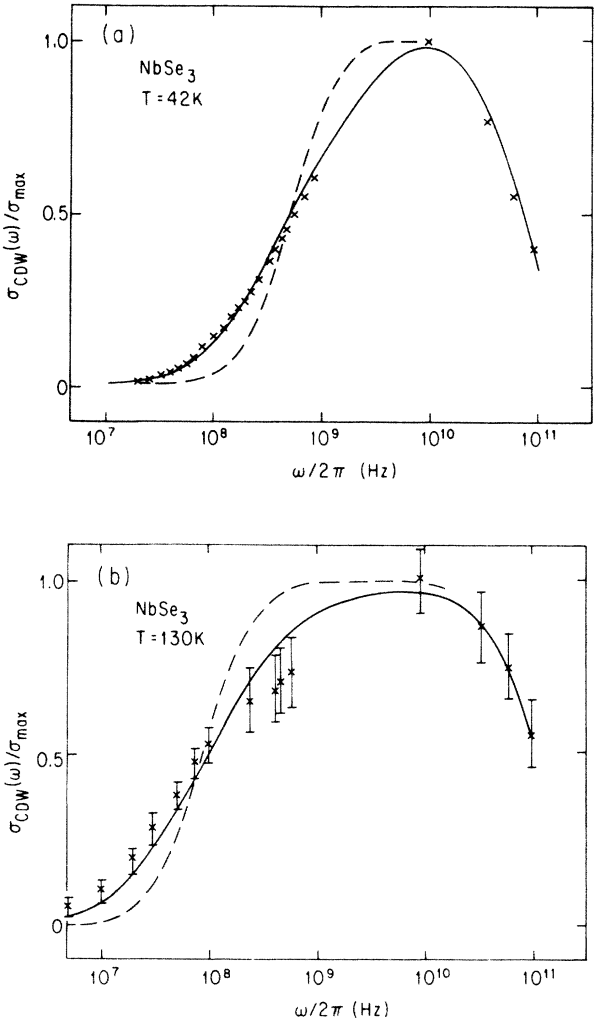

FIG. 11. $\mathrm{Re}\sigma_{\mathrm{CDW}}(\omega)$ normalized to the maximum conductivity versus frequency. The solid lines are a fit to Eq. (26) and the dashed lines are a fit to Eq. (15). The parameters are discussed in the text. (a) $T=42$ K with low-frequency results from Ref. 36. (b) $T=130$ K with low-frequency results from Ref. 37.

$$\sigma(\omega)=\frac{2}{\pi\omega_c}\int_0^\infty d\omega'\frac{1}{1+(\omega'/\omega_c)^2}\frac{\sigma_{\max}\omega^2}{\omega^2+\tau^2[\omega^2-(\omega')^2]^2}\ . \tag{27}$$

The parameters related to the damping, $\sigma_{\max}$ and $1/\tau$, do not follow a distribution in the second model. Including a distribution in the damping would broaden the response at higher frequencies as well as lower frequencies and not improve the fit. The distribution in ω_0 results in a broad response at frequencies below ω_c and only weakly affects the response at frequencies well above ω_c. The fit to this distribution still has three parameters, ω_c, $1/\tau$, and $\sigma_{\max}$, but fits the results to a much greater accuracy. For the fit in Fig. 11(a) the parameters are $\omega_c/2\pi=6.6$ GHz, $1/2\pi\tau=70$ GHz, and $\sigma_{\max}=25\,000\ (\Omega\,\mathrm{cm})^{-1}$. The presence of a distribution in ω_0 below or near 10 GHz in the second model does not affect the higher-frequency part of the harmonic oscillator fit and the two fits are almost identical in the inertial regime. In Fig. 11(b), the upper phase, the fit parameters are $\omega_c/2\pi=6$ GHz, $1/2\pi\tau=105$ GHz, and $\sigma_{\max}=2000\ (\Omega\,\mathrm{cm})^{-1}$, and this fit is also more accurate than the single oscillator model.

Fits to other distributions were attempted by replacing $(\omega_0/\omega_c)^2$ in Eq. (26) with $(\omega_0/\omega_c)^x$. For larger exponents ($x>2$) the distribution approaches a constant below ω_c with a sharp cutoff to zero at $\omega_0\simeq\omega_c$. This, however, results in a less adequate fit to the data because the few oscillators well above ω_c in Eq. (26) provide the unusual asymmetric shape of the calculated conductivity. For $x=1$ the distribution is not normalizable and the calculated conductivity is broadened at frequencies above 10 GHz, resulting in a fit interior to the fit from Eq. (27). Fits to fractional exponents were not attempted.

IV. CONCLUSIONS

We have observed a Drude-like conductivity at millimeter-wave frequencies in the CDW states of $NbSe_3$ and have used these results to determine the parameters which characterize the CDW response. The characteristic damping frequency observed, $1/2\pi\tau$, is 50 to 100 GHz in both CDW phases. The pinning frequency is less than 10 GHz, but a description in terms of a single oscillator response is not appropriate. A more accurate fit, with the same number of fit parameters, is obtained if the response is composed of a broad distribution of pinning frequencies; where the distribution is a constant well below some cutoff frequency and decreases to zero near the cutoff, rather than a single frequency. The effective mass m^*/m_e for the CDW response is approximately 230, well below the phase transition in the upper phase, and is approximately 100 in the lower phase. The lower-phase effective mass, deduced by treating the condensates from each transition as being strongly coupled, has a temperature dependence that is inconsistent with the mean-field theory even to low temperatures. This may indicate that the condensate from the lower transition is not rigidly coupled to the upper-phase condensate in the inertial regime. If a model is adopted, which treats the response in the lower phase as arising from two independent CDW's, then $m^*/m_e\simeq 95$ for the lower phase. These results

comprise the first determination of the complete set of response parameters for the dynamics of the CDW's in $NbSe_3$. A further discussion of these results may be found in II.

ACKNOWLEDGMENTS

The authors thank L. Mihaly, J. Bardeen, J. Tucker, S. Takada, and T. Holstein (deceased) for helpful discussions. We are indebted to Wei-Yu Wu and L. Mihaly for providing the low-frequency data and also thank B. Alavi and M. Maki for preparing the samples. The distributions fits were performed with the assistance of L. Mihaly. This research was supported by National Science Foundation Grants Nos. DMR-83-11843 and DMR-84-06896. One of us (D.R.) received financial support from IBM.

[1]See, for example, G. Gruner and A. Zettl, Phys. Rep. **19**, 117 (1985).
[2]P. A. Lee, T. M. Rice, and P. W. Anderson, Solid State Commun. **14**, 703 (1974).
[3]T. M. Rice, in *Low Dimensional Cooperative Phenomena,* edited by H. J. Keller (Plenum, New York, 1975).
[4]H. Fukayama and P. A. Lee, Phys. Rev. B **17**, 535 (1978).
[5]P. A. Lee and T. M. Rice, Phys. Rev. B **19**, 3970 (1979).
[6]P. Monceau, N. P. Ong, A. M. Portis, A. Meerchaut, and J. Rouxel, Phys. Rev. Lett. **37**, 602 (1976).
[7]G. Gruner, L. C. Tippie, J. Sanny, W. G. Clark, and N. P. Ong, Phys. Rev. Lett. **15**, 935 (1980).
[8]S. W. Longcor and A. M. Portis, Bull. Am. Phys. Soc. **25**, 340 (1980).
[9]J. C. Gill, Solid State Commun. **37**, 459 (1981).
[10]A. Zettl, C. M. Jackson, and G. Gruner, Phys. Rev. B **26**, 5773 (1982).
[11]J. H. Miller, J. Richard, J. R. Tucker, and J. Bardeen, Phys. Rev. Lett. **51**, 1592 (1983).
[12]Wei-Yu Wu, L. Mihaly, G. Mozurkewich, and G. Gruner, Phys. Rev. Lett. **52**, 2382 (1984).
[13]S. Sridhar, D. Reagor, and G. Gruner, following paper, Phys. Rev. B **34**, 2223 (1986).
[14]S. Takada, M. Wong, and T. Holstein, Phys. Rev. B **32**, 4639 (1985).
[15]D. Reagor, S. Sridhar, and G. Gruner, in *Charge Density Waves in Solids,* Vol. 217 of *Lecture Notes in Physics,* edited by Gy. Hutiray and J. Solyom (Springer-Verlag, Berlin, 1985), p. 155.
[16]S. Sridhar, D. Reagor, and G. Gruner, Phys. Rev. Lett. **55**, 1196 (1985).
[17]A. Zettl, G. Gruner, and A. H. Thompson, Phys. Rev. B **26**, 5760 (1982).
[18]L. I. Buravov and I. F. Schegolev, Prib. Tehk. Eksp. Instrum. Exp. Tech. (USSR) **14**, 171 (1971).
[19]J. A. Osborn, Phys. Rev. **67**, 351 (1945).
[20]S. Sridhar, D. Reagor, and G. Gruner, Rev. Sci. Instrum. **56**, 1946 (1985).
[21]J. Schwinger and D. Saxon, *Discontinuities in Waveguides* (Gordon and Breach, New York, 1968).
[22]N. Marcuvitz, *Waveguide Handbook,* MIT Rad. Lab. Series, (McGraw-Hill, New York, 1951), Vol. 10.
[23]J. A. Bradshaw, IEEE Trans. Microwave Th. Tech. **MTT-21**, 313 (1973).
[24]N. P. Ong and P. Monceau, Phys. Rev. B **16**, 3443 (1977).
[25]G. Gruner, A. Zawadowski, and P. M. Chaikin, Phys. Rev. Lett. **46**, 511 (1981).
[26]John Bardeen, Phys. Rev. Lett. **45**, 1978 (1980).
[27]R. M. Fleming, Phys. Rev. B **22**, 5606 (1980).
[28]M. Sato, H. Fujishita, S. Sato, and S. Hoshino, J. Phys. C **18**, 2603 (1985).
[29]R. M. Fleming, D. E. Moncton, and D. B. McWhan, Phys. Rev. B **18**, 5560 (1978).
[30]T. M. Rice, P. A. Lee, and M. Cross, Phys. Rev. B **20**, 1345 (1979).
[31]J. Stokes, A. N. Block, A. Janossy, and G. Gruner, Phys. Rev. Lett. **52**, 372 (1984).
[32]S. X. Tessema and N. P. Ong, Phys. Rev. B **23**, 5607 (1981).
[33]L. P. Gorkov and E. N. Dolgov, J. Low Temp. Phys. **42**, 101 (1981); E. N. Dolgov, Solid State Commun. **50**, 405 (1984).
[34]M. L. Boriak and A. W. Overhauser, Phys. Rev. B **15**, 2847 (1977).
[35]J. Bardeen, Mol. Cryst. Liq. Cryst. **81**, 1 (1981).
[36]Wei-Yu Wu, Ph.D. thesis, UCLA, 1985 (unpublished).
[37]G. Gruner, A. Zettl, W. G. Clark, and J. Bardeen, Phys. Rev. B **24**, 7247 (1981).